Advanced signal processing methods for pulsed laser vibrometry

Julien Totems,[1,*] Véronique Jolivet,[1] Jean-Philippe Ovarlez,[1] and Nadine Martin[2]

[1]Onera, The French Aerospace Laboratory, Theoretical and Applied Optics Department, Chemin de la Hunière, 91761 Palaiseau Cedex, France

[2]Gipsa-Laboratory, 961 Rue de la Houille Blanche, Domaine Universitaire, BP 46, F-38402 Saint-Martin d'Hères, France

*Corresponding author: julien.totems@onera.fr

Received 22 March 2010; accepted 27 May 2010; posted 10 June 2010 (Doc. ID 125828); published 8 July 2010

Although pulsed coherent laser radar vibrometry has been introduced as an improvement over its continuous wave (CW) counterpart, it remains very sensitive to decorrelation noises, such as speckle, and other disturbances of its measurement. Taking advantage of more polyvalent polypulse waveforms, we address the issue with advanced signal processing. We have conducted what we believe is the first extensive comparison of processing techniques considering CW, pulse-pair, and polypulse emissions. In this framework, we introduce a computationally efficient maximum likelihood estimator and test signal tracking on pseudo-time-frequency representations (TFRs), which, respectively, help deal with speckle noise and fading of the signal in harsh noise conditions. Our comparison on simulated signals is validated on a 1.55 μm all-fiber vibrometer experiment with an apparatus simulating vibration and strong speckle noise. Results show the advantage of the estimators that take into account actual noise statistics, and call for a wider use of TFRs to track the vibration-modulated signal.

OCIS codes: 280.0280, 280.3340, 120.7280.

1. Introduction

Coherent laser radars (lidars) are able to sense the small amplitude vibrations of remote surfaces, thanks to the Doppler effect. Long-range laser Doppler vibrometry has been successfully applied to an increasing number of situations where the goal is to determine the vibration characteristics of an inaccessible target. These applications range from structural assessment of potentially damaged buildings [1] to target identification for military purposes [2,3]. Although vibration frequencies and velocities are very different in magnitude, in both cases, the aim is to identify the modal frequencies of the target.

The measurement is performed as shown in Fig. 1. First, coherent heterodyne detection, done by mixing the Doppler-shifted backscattered laser wave and part of the emission (LO, local oscillator) on a detector, is the source of a heterodyne signal with an instantaneous frequency (IF) linked to the instantaneous velocity of the target surface. This heterodyne signal is frequency demodulated to retrieve the vibration velocity time series. Then the velocity time series is Fourier transformed and a vibration spectrum is obtained, which is analyzed to extract vibrational features. Interesting features include the modal frequencies of the target, appearing as peaks on the spectrum if the signal-to-noise ratio (SNR), between the peak power spectral density (PSD) and the noise floor PSD, is high enough.

In addition to continuous emission, a pulsed emission has been considered [3]. The simplest and most usual waveform is the pulse-pair, inherited from meteorological radars, processed by estimating the phase shift between the two consecutive pulses. At reception, each waveform provides one velocity sample of the time series. Polypulses were also tested [4].

0003-6935/10/203967-13$15.00/0

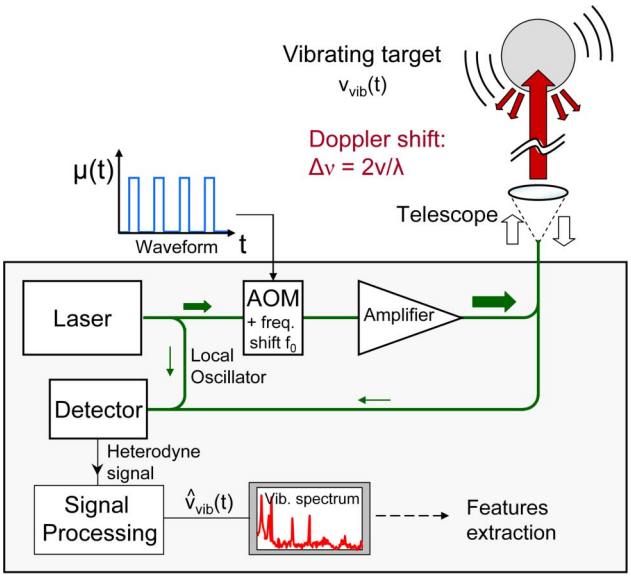

Fig. 1. (Color online) Diagram of a heterodyne coherent lidar vibrometer with a MOPA configuration, convenient for emitting arbitrary waveforms using the same AOM as for the frequency shift.

Pulsed vibrometry directly benefits from existing techniques in radar, for waveform design as well as signal processing.

The advantages of pulsed vibrometry have been discussed in [5,6]. First, a monostatic configuration of the vibrometer is easier to implement with static targets, because returns from the target can be temporally separated from parasitic reflections on the optics; having a single collimating optic in the instrument eases its pointing and focusing and might be required for compactness. Also, simultaneous telemetry by time-of-flight measurement becomes possible, allowing a time gating of the reception and the separation of multiple targets in the laser beam. Finally, higher peak power is available for the same average laser power, resulting in higher signal detectability and even slightly more accurate instantaneous Doppler shift estimation at a very long range.

Yet, as was shown by the comparison of CW and pulse-pair operation modes led by Hill *et al.* [6], the latter suffers from several drawbacks. When compared with the same mean emitted laser power, in normal noise conditions, the pulse-pair does not perform better than CW in obtaining good SNR on the final vibration spectrum. Each pulse-pair can yield slightly more accurate velocity estimates at a long range, thanks to a higher peak power, but with considerable averaging over numerous samples, CW mode still gets better results. Furthermore, strong phase noise, originating from speckle or laser phase noise, greatly decreases the pulsed mode performance, and pulse-pairs have an unambiguous velocity range only a few times larger than their velocity resolution.

In summary, past studies have concluded that despite its unique potential for very long range, multifunction, and monostatic instruments, pulsed vibrometry is impaired by its sensitivity to the disturbances of the measurement channel. However, the wide diversity of waveforms and signal processing available, compared to simple pulse-pair operation, indicates that performance improvement is possible. In this article, we investigate the potential of advanced signal processing techniques, applied to the polypulse waveforms already introduced in [4], which benefit from supplementary degrees of freedom. In the unfavorable conditions of strong speckle noise, we conduct an extensive performance comparison between CW, pulse-pair, and polypulse operation, processed by various classical and new processing techniques. The objective is to show how and to what extent pulsed vibrometry can be made more robust to harsh noise conditions.

Section 2 introduces the signal model and hypothesis. The characteristics of polypulse waveforms and known signal processing methods for CW and pulsed mode are recalled in Section 3. In Section 4, we propose and qualify new signal processing techniques for polypulse waveforms. We compare them to existing techniques, for the various waveforms, through simulation in Section 5. An experimental validation of this comparison, using an all-fiber vibrometer, is presented in Section 6. Section 7 concludes.

2. Signal Model

The photocurrent, downshifted from the carrier frequency f_0 to the null frequency, either analogically (I/Q demodulation) or digitally, is expressed, in a complex form:

$$\begin{aligned} i_S(t) &= \mu(t) i_{\text{het}}(t) + i_b(t) \\ &= \mu(t) i_0 m(t)\ \exp(j\varphi_{\text{vib}}(t)) + i_b(t), \end{aligned} \tag{1}$$

where $\mu(t)$ is the amplitude modulation applied to the laser emission in pulsed mode [$\mu(t) = 1$ in CW mode]; $i_{\text{het}}(t)$ is the heterodyne current, with a mean amplitude i_0; $m(t)$ is a complex multiplicative noise, circular and centered, with a variance set to 1; and $\varphi_{\text{vib}}(t) = 4\pi.x_{\text{vib}}(t)/\lambda$ is the phase modulation for the laser wavelength λ (1.55 μm) caused by $x_{\text{vib}}(t)$, the targeted surface vibration displacement projected along the laser line of sight. In case of a sinusoidal vibration, $x_{\text{vib}}(t) = a\sin(2\pi f_{\text{vib}} t + \varphi)$ and $v_{\text{vib}}(t) = 2\pi a f_{\text{vib}} \cos(2\pi f_{\text{vib}} t + \varphi) = V_{\max}\cos(2\pi f_{\text{vib}} t + \varphi)$. Lastly, $i_b(t)$ is an additive complex noise (detector and photon noise), white, Gaussian valued, circular, and centered, with variance ${\sigma_b}^2$. The time-averaged carrier-to-noise ratio (CNR) is defined as $\langle \text{CNR} \rangle = \langle |i_{\text{het}}|^2 \rangle / \langle |i_b|^2 \rangle = {i_0}^2 / 2{\sigma_b}^2$.

Complex multiplicative noise $m(t)$ contains amplitude and phase fluctuations terms and is the result of several phenomena [7]: speckle noise, laser phase noise, and the effect of atmospheric turbulence.

The random speckle pattern backscattered by the target is not static if the illuminated surface is moving, and as a consequence, the amplitude and phase of the received wave will vary, a phenomenon either called "speckle noise" or "target decorrelation noise"

in the literature [8]. The resulting multiplier has a complex normal distribution and autocorrelation function $\Gamma_m(\tau) = \exp(-\tau^2/{\tau_c}^2) = \exp(-{B_{\text{speckle}}}^2\tau^2)$. This means its phase and amplitude are roughly stable over durations shorter than $\tau_c = 1/B_{\text{speckle}}$ and that its frequency width is about $2\ B_{\text{speckle}}/\pi$. Depending on target distance and movement (target rotation has the largest impact), speckle bandwidth B_{speckle} varies in the 100 Hz–100 kHz range.

Laser phase noise is due to the finite spectral linewidth of the laser: as the emitted frequency is random, the frequency spread of the beat signal between the received wave and the LO increases as the target is further away and the waves become decorrelated. The result is a random phase term, of which the PSD can be predicted given the optical path difference. It can, however, be greatly mitigated by using a well-chosen delay line in the LO path.

Last, atmospheric turbulence, as an index distribution pushed across the beam by transverse wind, can also produce a complex multiplicative noise that affects both phase and amplitude; the characteristics of which have been inferred by Ishimaru [9]. Yet the phase term due to the turbulence piston is rather slow. Unless the laser beam is low above the ground, the amplitude fluctuations are slower than those due to target speckle, and turbulence noise is negligible in applications that involve moving targets.

Complex multiplicative noise impacts the measurement through signal fading (temporarily low CNR), as well as spectral broadening because of phase fluctuations, which directly lowers the accuracy of the velocity estimation.

The signal model of Eq. (1) is based on several simplifying hypotheses: (i) it is assumed that any bulk Doppler shift due to target global velocity has previously been removed; (ii) the illuminated surface vibrates as a whole, and no separate vibrators generate signals with various IFs; (iii) the target distance is known precisely (by means of simultaneous telemetry); (iv) the emitted mean laser power is equal for all operating modes, which implies taking $\langle \mu(t)^2 \rangle = 1$; and (v) lastly, we neglect the phase effects of atmospheric turbulence and laser phase noise and only consider speckle noise.

In that case, the noise parameters are the speckle bandwidth B_{speckle} and the CNR. B_{speckle} is set to 5 kHz (as induced by the parallax of a target with a 500 km/h velocity perpendicular to the line of sight of a laser radar with a 100 mm pupil). The vibration amplitude is chosen so that the modulation bandwidth is of the same order. Such values are consistent with the actual parameters expected for long-range moving vehicle identification (previous studies [6,8] considered speckle noise with lower bandwidth, a few hundred hertz). The CNR, averaged in time, is a common parameter for all operating modes, given the hypothesis of equal mean laser power in every case. It is calculated in the full sampling band of 1 MHz.

3. Background

A. Polypulse Waveforms

Pulsed waveforms are created by modulating the photocurrent amplitude by a square wave $\mu(t)$.

Because of the poor ambiguity-to-resolution ratio (i.e., measurement dynamic) offered by pulse-pair waveforms, we considered more general polypulse waveforms as was already done by Gatt *et al.* [4]. Though staggered polypulses present the highest measurement dynamic, in theory, their velocity ambiguities are difficult to solve in harsh noise conditions, and we focus, rather, on regular polypulses. As shown in Fig. 2, we define polypulses as a finite succession of N_p pulses of short duration t_p. These trains of pulses are repeated with period T, i.e., at pulse repetition frequency: $\text{PRF} = 1/T$. The pulses in the train are equally separated by duration T_S, and the total waveform duration is $T_m = (N_p - 1).T_S$.

We now discuss the constraints that apply on waveform parameters in order to choose a waveform best suited to given vibration and noise conditions.

One IF estimation (i.e., a velocity estimate) is performed for each polypulse. Its general principle is to differentiate the phase of singular pulses along the train, in order to obtain the IF, which is supposed constant during the short waveform duration T_m, chosen accordingly. The precision on this estimation is Fourier limited at approximately $1/T_m$, and, as a consequence, longer waveforms allow for better precision. But, when compared to a continuous wave of same effective duration, a polypulse waveform has the advantage that the energy is concentrated in pulses and the signal can be temporally separated from most of the noise affecting the measurement. In case of strong additive noise with the same energy, slightly better velocity precision is obtained in the pulsed mode. The downside is that Doppler ambiguities exist: velocity is known only within the ambiguity interval $V_a = \lambda/(2T_S)$.

The constraints for waveform design are the following: (i) the waveform repetition frequency PRF has to match the Nyquist criterion for the correct sampling of the vibration itself, $\text{PRF} > 2f_{\text{vib,max}}$, with $f_{\text{vib,max}}$ being the maximum significant vibration frequency of the target. (ii) T_S should be a function of the maximum velocity V_{max}, to remain in ambiguity interval V_a: $T_S \leq \lambda/(4V_{\text{max}})$. (iii) Depending on the

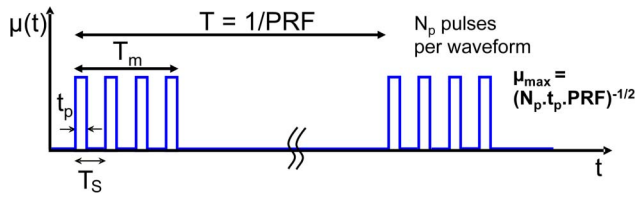

Fig. 2. (Color online) Parameters of polypulse waveforms in amplitude modulation $\mu(t)$: t_p, pulse duration; T_S, pulse separation; T_m, polypulse duration; PRF, waveform repetition frequency; N_p, pulse number per waveform; and μ_{max}, maximal amplitude of $\mu(t)$.

required velocity accuracy, N_p should then be chosen so that the effective duration of the waveform $\sigma_t = \int t^2.\mu(t)\mathrm{d}t$, roughly proportional to N_p, allows a small enough velocity resolution $\delta V = \lambda/8\pi\sigma_t$, while satisfying the hypothesis of a stationary IF during the waveform duration. Polypulses indeed provide a larger measurement dynamic (linear) $D = V_a/\delta V$ than pulse-pairs: $D_{2\text{pulses}} \approx 9$, while $D_{4\text{pulses}} \approx 28$, for instance.

Those three fundamental constraints are set according to the expected vibration, for which coarse assumptions can be made by knowing the nature of the target. Beyond this essential adaptation to the vibration, actually optimizing waveform parameters relies on other variables, such as the noise conditions. In fact, the optimal pulse number N_p is very dependent on the relative power of the signal and noise, as well as the correlation time of the phase of the signal, due to phase noise. Indeed, the duration of the polypulse should remain shorter than this correlation time. Such as in [6], we choose to compare waveforms by setting the same mean laser power for all, in order to avoid taking into account the evolving limitations of lasers and benefit from a common ground to evaluate the efficiency in spending a given energy for the measurement. This hypothesis implies that, this energy being equally divided into the N_p individual pulses, their peak power decreases as N_p is increased. Simple considerations led us to choose $N_p = 6$ (above which velocity resolution stalls because of IF nonstationarity) and PRF $= 500$ Hz (just above Nyquist's criterion for a 200 Hz maximum vibration frequency) in our study.

B. Signal Processing for Coherent Laser Radar Vibrometry

In this subsection, we recall signal processing strategies for vibrometry and present the estimators that are compared in Section 6.

The goal of the measurement is to determine the vibration velocity by IF estimation, in order to evaluate modal frequencies of vibration, whereas detection noise, phase noise, and fading disturb this estimation. Two main strategies stand out: (i) phase differentiation over samples (in CW) or pulses, such as in conventional frequency demodulation, (ii) spectral maximum estimation or time-frequency processing, which works by determining the frequency localization of the maximum of energy along time, on a time-frequency representation (TFR), such as a spectrogram [10]. Parametric estimation, based on a full signal model, is a third possible way, supposedly optimal [6,11], but never applied it because of its complexity. We have not considered this approach in this paper.

The vibration velocity is usually Fourier transformed to identify peaks at potential modal frequencies, which are the actual data of interest. A relevant performance indicator is then the SNR, the PSD ratio between the peak and the noise spectrum. For completeness, we mention there are variations for this last step of the process, such as the parametric estimation of the vibration modes given the preevaluated noise variance [12].

1. *Instantaneous Frequency Estimators in CW Mode*

The sliding "coherent average" of phase differences between K consecutive samples is an enhancement of pulse-pair processing [6]. This estimator, presented in Table 1, belongs to the phase differentiation family defined earlier and is called autocorrelation first lag (AFL).

The following two techniques use a TFR; the spectrogram is here preferred to better performing kernels, such as the Born–Jordan [11], because of its much shorter computation time. First, we implement the centroid of the spectrogram columns [7], with a circular sum in order to avoid bias from the nonzero-mean noise background [spectrogram centroid (SGC)]. But the spectrogram can also be processed using a spectral equivalent of the phase-based estimator originally given by Lee, as explained in [13,14]. Lee's spectral matching (LSM) consists of finding the best match in position between a reference spectrum $S_{\text{ref}}(f)$ (Gaussian spectrum induced by the speckle noise) and the short-term spectra composing the spectrogram.

Centroid-based (SGC) and Lee (LSM) estimators allow a large improvement over the simple maximum detection over time on a TFR, especially when strong complex multiplicative noise is involved and when compared to other frequency estimators [10,14]. The AFL estimator is also interesting, as calculation and comparison show that it is, in fact, equivalent to SGC, without, however, the advantages of time-frequency analysis introduced in Section 4.

2. *Instantaneous Frequency Estimators in Pulsed Mode*

In the pulse-pair mode, the fourth estimator of Table 1 uses the phase difference between each pair of pulses [pulse-pair (PP) estimator]. Telemetry data or previously performed pulse detection is necessary in order to properly window the signal. This method is straightforwardly extended to polypulse waveforms: the phase difference between consecutive pulses is coherently averaged [polypulse pair (PPP) estimator]. This estimator is the fastest of those applied to polypulses. But several authors, as in [14,15], insist on the benefit of phase differentiation over nonconsecutive pulses.

The autocorrelation Fourier transform (AFT) estimator thus performs a linear regression of the autocorrelation function phase, i.e., the search of the Fourier transform (FT) maximum, after a proper windowing. In order to take into account the decorrelation induced by speckle noise, and to avoid using uncorrelated pairs of pulses, the windowing function $h(\tau)$ is set to the modulus of $\Gamma_{is,k}(\tau)$, averaged on all polypulses.

Table 1. Implemented Instantaneous Frequency Estimators

CW mode	AFL	$\hat{f}_{\text{inst}}(t) = \frac{1}{2\pi\Delta t}\arg\left(\sum_{n=1}^{N_m} i_s(t+n.\Delta t) i_s{}^*(t+(n-1).\Delta t)\right)$	(2)	Δt, sampling period; n, sample index; N_m, number of samples for IF estimation
	SGC	$\hat{f}_{\text{inst}}(t) = \frac{B_a}{2\pi}\arg\left(\int_{Ba} \lvert\text{STFT}(t,f)\rvert^2.\exp\left(j2\pi\frac{f}{B_a}\right)\mathrm{d}f\right)$	(3)	B_a, analysis bandwidth; $\lvert\text{STFT}(t,f)\rvert^2$, spectrogram
	LSM	$\hat{f}_{\text{inst}}(t) = \arg\max_f(S_{\text{ref}}(f) \otimes \lvert\text{STFT}(t,f)\rvert^2)$	(4)	$S_{\text{ref}}(f)$, reference spectrum
Pulsed mode	PP	$\hat{f}_{\text{inst}}(t = k/\text{PRF}) = \frac{1}{2\pi T_S}\arg(\langle i_s\rangle_{k,2}\langle i_s\rangle^*_{k,1})$	(5)	k, waveform index; $\langle i_s\rangle_{k,p}$, signal average over pulse #p of waveform #k
	PPP	$\hat{f}_{\text{inst}}(t = k/\text{PRF}) = \frac{1}{2\pi T_S}\arg\left(\sum_{p=2}^{N_p}\langle i_s\rangle_{k,p}\langle i_s\rangle^*_{k,p-1}\right)$	(6)	
	AFT	$\hat{f}_{\text{inst}}(t = k/\text{PRF}) = \arg\max_f\left(\left\lvert\int \arg(\Gamma_{i_s,k}(\tau)).h(\tau).\exp(-j2\pi f\tau)\mathrm{d}\tau\right\rvert\right)$	(7)	$\Gamma_{is,k}(\tau)$, autocorrelation of polypulse #k; $h(\tau)$, weighting function
	MF	$\hat{f}_{\text{inst}}(t = k/\text{PRF}) = \arg\max_f\left(\left\lvert\int_{\text{Polypulse \#}k} i_s(t').\mu(t').\exp(-j2\pi f t')\mathrm{d}t'\right\rvert\right)$	(8)	Radar MF

The matched filter (MF) approach, as in radar processing, equivalent to the previous one when $h(\tau) = 1$, uses the spectrum of the received waveform multiplied by the emitted waveform (MF). It can be applied to any waveform. With only additive white noise, this estimator is the maximum likelihood (ML) estimator, asymptotically optimal at high CNR.

4. Advanced Instantaneous Frequency Estimation with Polypulse Waveforms

A. Maximum Likelihood Instantaneous Frequency Estimation

In coherent laser radar multiplicative noise is also present. We thus propose the actual ML estimator of the IF of a received polypulse, given the signal model of Eq. (1). We assume stationary waveforms and prior knowledge of the noise parameters.

For faster computation, the likelihood is calculated by applying a variable change proposed by Ghogho *et al.* in [16]. It uses the fact that if the phase of the signal can be factored, what remains is the sum of multiplicative and white additive noises, which have known statistics. The resulting polypulse IF ML estimator is

$$\hat{f}_{\text{inst}}(t = k/\text{PRF}) = \arg\max_f((\vec{s}')^T Q_{s'}^{-1}(\vec{s}')), \quad (9)$$

with

$$\vec{s}'(p) = \langle i_s\rangle_{k,p}\exp(-j2\pi f.pT_S) \quad \text{for } p = 1,\ldots,N_p,$$
$$Q_{s'} = \text{CNR}_{\text{peak}}Q_m + I_{N_p}, \quad (10)$$

where $Q_{s'}$ is the sum of the noise covariance matrices, as sampled by the pulses; Q_m is the covariance matrix of multiplicative noise m; and I_{N_p} is the identity matrix. Element (p,q) of Q_m is given by the autocorrelation function of the considered multiplicative noise, in our case, speckle:

$$Q_m(p,q) = Q_{\text{speckle}}(p,q) = \Gamma_{\text{speckle}}((p-q)T_S)$$
$$= e^{-B^2_{\text{speckle}}T_S^2(p-q)^2} \quad \text{for } p,q = 1,\ldots,N_p. \quad (11)$$

ML is the equivalent of the Levin ML estimator developed for CW laser radar, explained in [13], but applied to polypulse waveforms. As the Levin estimator does in the spectral domain, when the phase modulation of the signal is suppressed assuming the IF was f, this likelihood quantifies how much the result is close to having the same covariance matrix as the supposedly remaining multiplicative and additive noises. Like the MF, it can also be seen as a linear regression of the phase: the scalar product with $\exp(-j2\pi ft)$ is calculated on a series of correlated pulses selected by ${Q_{s'}}^{-1}$, and averaged over the considered series. Note that, in fact, when B_{speckle} tends toward zero, the ML estimator becomes equivalent to the MF.

The ML estimator is theoretically optimal if the signal model of Eq. (1) is verified, but it might not perform as well under strong noise conditions (low CNR or very high B_{speckle}) or in the case of deviations from the model. Also, knowledge of the noise parameters CNR and B_{speckle} is necessary in order to use this estimator. Both of them can be evaluated by studying the amplitude of the signal: CNR via the ratio of power in and out of the pulses and B_{speckle} by calculating the width of the autocorrelation function of amplitude fluctuations. A third, more direct, method is to evaluate $Q_{s'}$ from the signal, demodulated by a quick coarse IF estimate. This can be written as

$$\hat{Q}_{s'} = \sum_{k=1}^{K}\vec{s}'_k.\vec{s}_k{}'^T \quad \text{with} \quad \vec{s}'_k(p)$$
$$= \langle i_s\rangle_{k,p}\exp(-j2\pi\hat{f}_k.pT_S) \quad \text{for } p = 1,\ldots,N_p, \quad (12)$$

where K is the total number of waveforms during the measurement and f_k is the coarse estimate previously obtained for waveform #k. The PPP estimator is fast enough to provide this estimate.

The proposed ML estimator can be modified in case the noise characteristics differ from those of our primary model; for instance, if there is laser frequency noise in addition to the speckle noise in $m(t)$, then Q_m becomes the elementwise product of Q_{speckle} and Q_{laser}, also given by the autocorrelation function of the laser phase noise, found in [17].

B. Performance of Maximum Likelihood Estimator

In order to assess the performance of the ML estimator, the Cramér–Rao lower bound (CRB) of the velocity estimation over each received polypulse waveform is calculated from the likelihood function, without variable change and pulse average:

$$\sigma_v \geq \frac{\lambda}{2}\left[\mathrm{Tr}\left(\left(\frac{\partial Q}{\partial f}Q^{-1}\right)^2\right)\right]^{-1/2}, \tag{13}$$

in which Tr() designates the matrix trace operation and Q is the covariance matrix of the nonzero samples of the signal, with elements

$$Q(u,v) = \mu_{\max}^2 i_0^2 \Gamma_m((u-v)\Delta t)e^{j2\pi f(u-v)\Delta t} + \sigma_b^2\delta(u-v), \tag{14}$$

for $u, v = 1, \ldots, N_w$ so that $\mu(u)\mu(v) \neq 0$, where Δt is the sampling period and N_w is the number of samples in the total duration of one polypulse waveform: $T_m + t_p$.

This CRB can be evaluated numerically and is found to agree with the analytical expression in case of only additive noise [13]:

$$\sigma_v \geq \frac{\lambda}{4\pi\sqrt{2}\sigma_t}\frac{\sqrt{\mathrm{CNR}_{\mathrm{wf}}+1}}{\mathrm{CNR}_{\mathrm{wf}}}, \tag{15}$$

in which $\mathrm{CNR}_{\mathrm{wf}}$ is the CNR taken in terms of waveform energy: $\mathrm{CNR}_{\mathrm{wf}} = E_{\mathrm{waveform}}/\mathrm{PSD}_{\mathrm{noise}}$ (E_{waveform}, waveform energy; $\mathrm{PSD}_{\mathrm{noise}}$, power spectral density noise).

As described in [7], error saturation and fading have to be taken into account. The resulting error after fading is, indeed, the quadratic sum of the CRB at given CNRs weighted by the probability of this CNR occurring (Rayleigh law). This probabilistic inclusion of fading helps better predict the error but may affect the lower bound property.

Figure 3 shows velocity error as a function of CNR with PP, PPP, and ML estimators and CRBs on simulated signals, assuming a nonvibrating target and a 5 kHz bandwidth speckle noise. We inject the real values of CNR and B_{speckle} in the ML estimator.

In the pulse-pair mode, theory predicts a limit for the velocity precision at high CNR, due to the predominant complex multiplicative noise. PP processing on a simulated signal shows the expected plateau related to this phenomenon, but much higher than expected. For this reason, we can suspect PP processing may not be optimal.

For six-pulse waveforms, Fig. 3 shows a globally lower velocity error. At high CNR, the CRB does not saturate and decreases, which is not the case with PPP processing, as decorrelation between pulses impacts the velocity estimation. On the other hand, ML processing follows the bound and achieves velocity precision of about 0.2 mm/s instead of 0.5 mm/s with PPP and 2 mm/s with pulse pairs, at high CNR. Indeed, when the measurement is predominantly affected by complex multiplicative noise, i.e., at a high CNR, the ML estimator performs better than PPP, for any value of B_{speckle}.

The ML estimator is robust to the CNR and B_{speckle} parameters. For signals with CNR = 20 dB and B_{speckle} = 5 kHz and varying parameter inputs for the ML estimator, performance is not significantly affected unless B_{speckle} or CNR is misestimated by several kHz and tens of dB, respectively. As the estimation of these parameters on the amplitude of the signal provides very accurate values compared to such requirements, in the conditions where the ML estimator is useful (B_{speckle} of a few kHz, CNR > 0 dB), no problem should arise from the strategy of preestimating noise parameters. If it should prove difficult in practice, we are still able to evaluate the covariance matrix of the noise, after a fast PPP demodulation of the signal that would allow us to reconstitute a vibration-suppressed signal containing only noise.

Finally, we have investigated the modification of the ML estimator for laser phase noise incorporated in the signal model, using the autocorrelation predicted by [17] for a narrow linewidth laser [18]. In that case, we notice that while six-pulse waveforms still bring general precision improvement over pulse pairs, ML processing does not provide much smaller velocity error than PPP, except for predominant

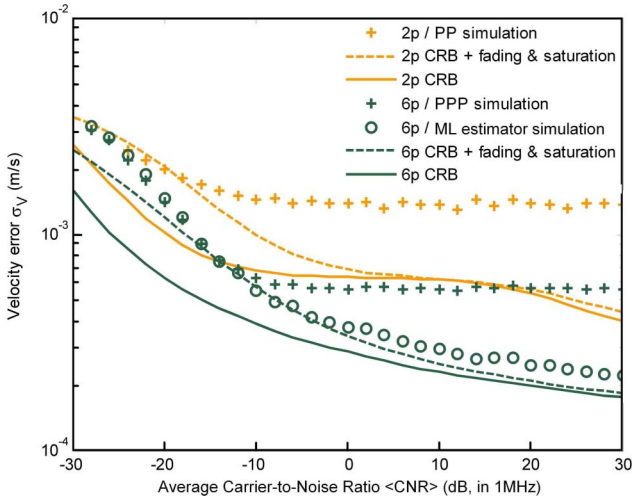

Fig. 3. (Color online) Comparison of velocity errors of PP, PPP, and ML estimators and theoretical CRB for the velocity error, as a function of average CNR, for the pulse pair ($2p$) and six-pulse ($6p$). Two thousand simulated waveforms with $T_S = 50\,\mu$s and $t_p = 2\,\mu$s at $B_{\text{speckle}} = 5$ kHz. Only the ML estimator reaches the CRB.

speckle noise as we have already seen, and moderate decorrelations (optical path difference well below laser coherence length). When the correlation time of the signal is under pulse separation T_S, the CRB quickly rises and both PPP and ML estimators stick to that bound.

We conclude that the ML estimator is interesting to implement in order to make pulsed vibrometry less sensitive to decorrelation, such as that produced by target speckle. The remaining velocity error approaches the CRB when CNR is high, which indicates it is close to optimal for the signal model of Eq. (1). Noise parameters are required as inputs and can be previously estimated on the signal amplitude. The impact of laser phase noise cannot be mitigated as much, certainly because the correlation time of the signal easily falls below T_S. We must finally stress that deviations from the signal model are well known to affect ML estimators. For instance, high-frequency vibrations cause the IF to drift even within the short duration T_m of the polypulse, in which case ML processing as we designed it here will not perform as well.

This preliminary qualification is, however, incomplete without a thorough comparison to other estimators from literature on actual vibration signals, which is presented in Section 5.

C. Time-Frequency Representation in Pulsed Mode

Another way of improving signal processing in pulsed vibrometry is to perform signal tracking on a TFR, in order to compensate for the small number of measurements. A great gain over nontracking methods is expected. At low CNR, it will avoid outlying values of velocity due to a temporarily weak signal. Also, multiple components caused by several vibrating parts of the target could be separated. The downside is that TFR processing is more demanding in computation time and memory.

In the pulsed mode, a TFR can be drawn for the three estimators we proposed in this article. MF (radar matched filter), AFT (see Table 1), and the ML estimator all rely on the search of a frequency maximum, whether it is a spectrum or a log-likelihood function, for each received waveform. We propose to track the frequency localization of the maxima of energy for noise mitigation at low CNR. We build a two-dimensional representation with, as coordinates, frequency and waveform number, which can be linked to instants in time. Figure 4 shows examples of what can be obtained on simulated signals.

From a five-tone vibration with maximum velocity of about 6 mm/s, we simulate the heterodyne signal according to the model of Eq. (1). The average CNR (in the 1 MHz bandwidth) is chosen as low as −20 dB to show the phenomenon of spurious peaks that come from temporarily strong noise or weak signal, and strong speckle noise of bandwidth $B_{\text{speckle}} = 5$ kHz is applied. Six-pulse waveforms with $t_p = 2\,\mu$s, $T_S = 50\,\mu$s, and PRF = 500 Hz are used. For ML we choose a $1/3T_m$ frequency step, and for MF and AFT, which are based on fast FTs, zero-padding is applied to provide a similar resolution. Also, for better visibility, the plotted function is the normalized likelihood function, instead of the log-likelihood of Eq. (9). The functions for each waveform are plotted within the ambiguity range $[-1/2T_S; 1/2T_S] = [-10\,\text{kHz}; 10\,\text{kHz}]$. On the left side of these charts, there is no additional processing. The frequency-modulated signal is seen as a discontinuous trace, which produces a very noisy velocity time series if processed by maximum picking or even by centroiding.

The interest of TFR is highlighted here, as the correct vibration trace is still visible, despite isolated peaks originating from the noise, whereas standard algorithms give a velocity time series corrupted by many outliers. We use an IF continuity hypothesis on the pseudo-TFR in order to better extract the vibration in case of strong noise conditions, which should especially benefit our ML processing, inherently inclined to be affected in such a case.

A number of techniques are available that take advantage of the continuity of the signal trace [19,20]. We choose, rather, a simple temporal smoothing of the TFRs, as is done on the right side of Fig. 4. The lines of the TFR have been low-pass filtered, with a bandwidth preserving the higher frequencies of vibration. If a few consecutive waveforms detect slowly drifting IF, due to the frequency spread the energy is integrated, whereas transitory peaks from the noise are smoothed. Such regularization allows a better recovery of the vibration velocity time series by a subsequent maximum picking or centroiding, especially in the case of ML processing, as will be seen in the next section.

In our comparative simulations of processing methods and waveforms, we applied temporal smoothing to MF-, AFT-, and ML-generated TFRs, and also to TFRs in CW mode, for a fair comparison. The methods are then annotated accordingly (with smoothing): MF-s, AFT-s, ML-s, SGC-s, LSM-s.

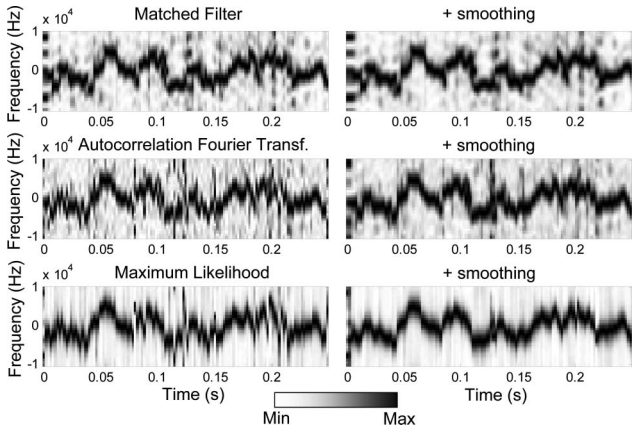

Fig. 4. TFRs obtained for simulated signals (six-pulse waveforms, PRF = 500 Hz, $T_S = 50\,\mu$s, and $t_p = 2\,\mu$s) with matched filtering, AFT, and ML at low CNR (−20 dB in 1 MHz) and $B_{\text{speckle}} = 5$ kHz. On the right side, temporal smoothing of the TFRs brings out the vibration trace.

5. Comparative Simulation of Processing Methods in Pulsed and Continuous Wave Mode

We now study the performance of the advanced processing techniques that were introduced in Section 4, relative to the existing methods presented in Section 3. This comparison is conducted on realistic signals with additive detection noise and complex multiplicative speckle noise and with a vibration comprising several modes. In this section, the study is based on simulated signals.

The simulation relies on the model developed in Section 2. Subroutines generate the complex phasor induced by the vibration as well as additive and multiplicative noises, which are resampled as suitable for each type of waveform and used to produce the signal. The same mean power hypothesis is taken into account as a normalization of the signal amplitude.

Using simulated heterodyne signals, we qualify all presented processing methods on the criterion of SNR, which is evaluated on the vibration spectrum, as the ratio of the PSD at the peak frequency of interest over the PSD of the noise floor. The PSD is estimated using the periodogram. The simulated vibration has five peak frequencies between 8 and 120 Hz, and the maximum velocity is over 5 mm/s. The retained SNR value is the average of the five individual SNRs. For each given result, we average the SNR values obtained in 200 signal realizations.

The wavelength is $\lambda = 1.55\,\mu$m; measurement duration is $T_{\mathrm{mes}} = 1$ s, with sampling frequency $f_{\mathrm{ech}} = 1$ MHz in CW, and 2 MHz in pulsed mode. In pulsed mode, the modulation parameters are $N_p = 2$ (pulse pairs) or $N_p = 6$ (six-pulse), $t_p = 2\,\mu$s, $T_S = 50\,\mu$s and PRF = 500 Hz, which is a little above the Nyquist criterion for the correct sampling of the vibration. The analysis bandwidth in which the IF estimation is performed, both in CW and pulsed mode, is $B_a = 20$ kHz, corresponding to ± 7.75 mm/s at our working wavelength. B_a is thus closely adapted to the signal bandwidth induced by vibration and speckle. The spectrogram and autocorrelation window duration in CW mode is chosen as 1/PRF = 2 ms. The CNR is still given in average in a 1 MHz bandwidth for CW mode (noted ⟨CNR⟩); for comparison, the peak CNR in pulsed mode, in the reduced analysis bandwidth, is greater by 17 dB ($6p$) or 27 dB ($2p$). The speckle noise bandwidth is $B_{\mathrm{speckle}} = 5$ kHz.

Figure 5 shows vibration spectra averaged over 200 runs, obtained at a high CNR: 30 dB. Only the best results for each waveform are plotted. The five vibration peak frequencies are visible on each curve and can be identified. However, the noise floor is much lower with polypulse waveforms and the ML estimator with smoothing (ML-s), or with CW and SGC-s, than with pulse pairs, which remain the most sensitive to the strong speckle noise applied in this simulation. In that case, pulse-pair operation cannot detect vibration modes with peak velocities under

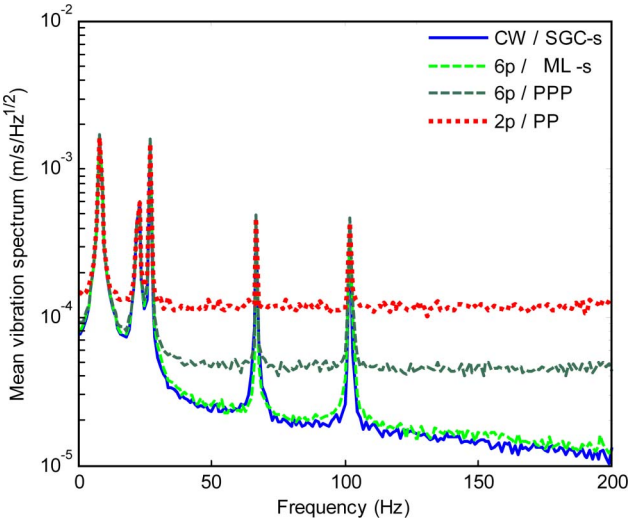

Fig. 5. (Color online) Average vibration spectra simulated at a high CNR (30 dB in 1 MHz) processed by the estimators giving the best SNR for CW, pulse pairs ($2p$), and six-pulse waveforms ($6p$). The noise floor is much lower with the ML estimator than with the PPP estimator.

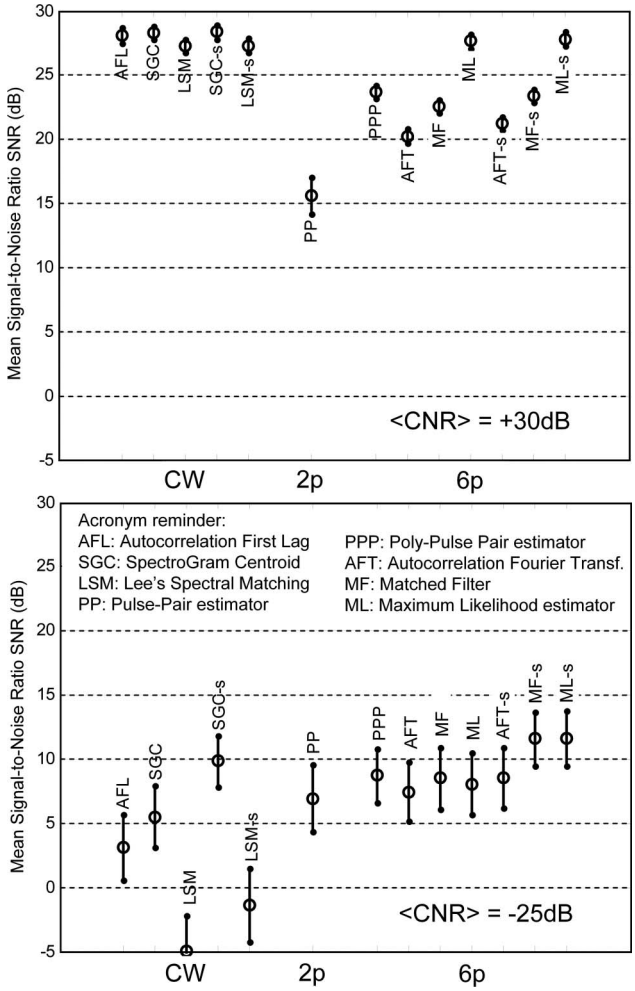

Fig. 6. Average SNRs obtained in simulation at $B_{\mathrm{speckle}} = 5$ kHz and high CNR [(top)30 dB] or low CNR [(bottom) −25 dB] for CW, pulse pairs ($2p$), and six-pulse waveforms ($6p$). The suffix "-s" denotes smoothing is applied on the pseudo-TFR obtained using the preceding estimator.

Table 2. Computation Times for Implemented Estimators[a]

Method	AFL	SGC	LSM	PP	PPP	AFT	MF	ML
Computation time (s)	0.9	1.5	1.1	10^{-3}	10^{-3}	0.97	0.18	0.17

[a]These results were obtained with MATLAB on a 2.13 GHz CPU.

0.1 mm/s, contrary to polypulses with advanced processing.

A more detailed comparison in terms of SNR results for all processing methods is presented in Fig. 6 at a high CNR (top) and at a very low CNR (bottom). The mean SNR of each method is plotted as well as its standard deviation over the 200 runs.

At a high CNR ($\langle \mathrm{CNR} \rangle = 30$ dB) when speckle noise is predominant, all processing methods in CW mode perform equivalently well, whereas important differences appear between the various techniques applied to the pulsed mode. First, pulse-pair SNR is more than 10 dB worse than the best results obtained with six-pulse waveforms or in the CW mode. Better averaging of the phase noise with "longer" waveforms is the reason of such a difference. We also find an average 5 dB higher SNR given by the ML estimator proposed here, compared to the other estimators, including the commonly used radar MF. However, it should be noted that CNRs over 15 dB are scarcely encountered, and, in practice, this gain may remain limited (see Section 6). The PPP estimator offers relatively good performance (on top of a low computational load) because it only relies on pairs of consecutive samples, which have less chance of being decorrelated, whereas standard spectral estimators look for a global phase trend, more easily corrupted when ambiguities are possible.

At a very low CNR ($\langle \mathrm{CNR} \rangle = -25$ dB in 1 MHz), it is known that without speckle noise, high peak power waveforms (such as pulse pairs) allow slightly better SNR on the measured vibration spectrum. In this simulation, however, because speckle noise is strong, there is no such gain. In CW mode, spectrogram centroiding allows the best SNR, while LSM is badly affected by strong detection noise. With polypulse waveforms, all estimators are roughly equivalent. Temporal smoothing benefits more to spectrogram processing in CW (5 dB gain) than to ML and MF processing with polypulses (3 dB gain). This is because of the lesser number of averaged columns of the pseudo-TFR in pulsed mode. We also note that ML and MF are equivalent when the effects of speckle noise are not predominant.

The results obtained at a medium CNR are intermediary. The usual plateau at a higher CNR starts at $\langle \mathrm{CNR} \rangle = -5$ dB. However, ML performance does not stall and increases slowly with CNR.

The computational load of the various processing methods is summarized in Table 2. Attention is called to the following results: pulse-pair-based estimators are practically immediate compared to all other estimators and can provide an initial estimate of the vibration velocity; for more complex estimators that would be employed afterward. The ML estimator is the fastest spectral estimator used here. MF is equivalently fast. SGC remains the best but also the heaviest estimator in this study. As expected, pulsed vibrometry is faster to process in general, due to a fewer number of samples.

We now conduct another performance simulation with a varying analysis bandwidth B_a, that was previously fixed at 20 kHz to match the vibration bandwidth. This assumption was, in fact, very restrictive because, in practice, the bandwidth of the vibration is unknown, so T_S and thus $B_a = 1/T_S$ have to be chosen large enough so that no velocity ambiguity is possible. Yet bandwidth adaptation is important at low CNR so as to avoid letting too much additive detection noise in the IF estimators.

All other simulation parameters remaining the same, in Fig. 7, we plot SNR results obtained at a low CNR (−20 dB) when bandwidth adaptation matters the most as a function of the bandwidth adaptation parameter $\alpha = B_a/B_{\mathrm{vib}}$, where B_{vib} is the vibration-induced frequency excursion. It shows that SNR is very dependent of the analysis bandwidth. When $\alpha < 1$, as expected, signal losses and Doppler ambiguities deteriorate the measurement, especially in pulsed mode, for which an α slightly above one is preferable to avoid ambiguities. But for $\alpha > 1$, the various estimators react differently to the more important noise accepted in the analysis bandwidth. Temporal smoothing in both the CW and pulsed modes is necessary to avoid a fall of SNR beyond $\alpha = 2$. For instance,

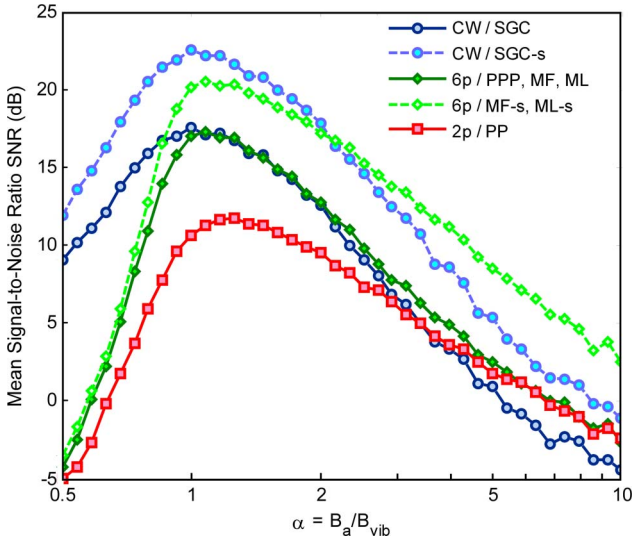

Fig. 7. (Color online) Average SNRs at low CNR (−20 dB) plotted as a function of the ratio between analysis bandwidth B_a and vibration bandwidth B_{vib}, for CW, pulse pairs ($2p$), and six-pulse waveforms ($6p$).

for a 100 kHz analysis bandwidth, i.e., $T_S = 10\,\mu$s and $\alpha = 5$, only pulsed mode with polypulse waveforms processed by ML or MF and pseudo-TFR temporal smoothing is able to retain around 10 dB SNR. In some conditions, even with strong speckle noise, pulsed mode as enhanced by the methods described in this article can be preferable because of its robustness to additive noise.

6. Experimental Validation

A. Apparatus

In order to confirm the results of Section 5, an all-fiber 1.55 μm vibrometer was implemented, with the configuration described in Fig. 8. Fibered systems with a master oscillator power amplifier (MOPA) configuration are an interesting choice in this case because of their compactness, ease of use, and versatility; switching from CW emission to pulsed emission only requires applying a modulation on the driving signal of the acousto-optic modulator (AOM) used for frequency shifting of the emitted laser wave.

Separate optics were used for emission and reception, which is essential in CW mode on static targets. The output waveforms were monitored because the amplifier distorts the input impulsions and the modulating signal needs to be adjusted in compensation. The laboratory experiment also includes an apparatus to create the same vibration as the one used in Section 5 and to produce speckle noise with the controllable characteristic B_{speckle}, while the CNR can be acted upon via a tunable attenuator placed before the emission optics.

The optical beam from a Koheras laser injector delivering 10 mW with 90 kHz linewidth is split into a signal beam and a LO beam. The signal wave is modulated by an IntraAction AOM frequency shifter at 70 MHz. Its driving signal can be amplitude modulated in pulsed mode by a digital gating signal that provides the waveform frame and an analog signal, generated by a Wavetek arbitrary waveform generator, which allows the fine tuning of the emitted power over time. Both signals are necessary to ensure correct extinction of the emission. The modulated optical wave is then fed into a Keopsys 1 W erbium-doped fiber amplifier (EDFA) operated at 100 mW output. The power is sent to the emission telescope but can be attenuated to vary the CNR. The emitted wave reflects on the vibrating mirror, a few meters away, and is scattered by a rotating diffuse target. The rotation rate of the target sets the speckle bandwidth B_{speckle}. A second telescope receives this backscattered wave, which is mixed with the LO on a Hamamatsu InGaAs detector with a 100 MHz bandwidth.

The heterodyne signal, around 70 MHz, is amplified and frequency downshifted by mixing it with the 67.5 MHz output of a HF generator. The resulting signal, with 2.5 MHz intermediate frequency, is low-pass filtered at 5 MHz and digitized on 16 bits at a 15 MHz sampling frequency, by a National Instruments 5922 acquisition card (ADC).

Signal processing is then implemented on MATLAB, for 1 s duration acquisitions. The analytic signal (complex signal around null frequency) is derived by a Hilbert transform of the acquisition and is either decimated to 1 MHz sampling frequency in CW mode, or pulse averaged in the pulsed mode. Both of these methods allow useful data reduction. Finally, the processing methods discussed in this study are applied to determine the vibration spectrum of the mirror, and performance in terms of SNR is calculated by the same means as in Section 5.

The parameters t_p, T_S, and PRF of the waveforms are also roughly identical to the ones chosen previously. As expected, the amplitude modulation applied on the AOM driving signal has to be precompensated in order to obtain a suitable waveform amplitude function $\mu(t)$, because of EDFA-related phenomena [21]. In order to avoid having to retune this precompensation as we switch from one waveform type to another, the pulse-pair mode is implemented by simply taking the first two pulses of the six-pulse waveforms. After a preliminary calibration of average CNR in regard to output power in the several emission modes, we vary the power attenuation at the emission in order to study the SNR given by each estimator at various CNR values. The speckle bandwidth induced by the rotating disk is set to approximately 5 kHz, as verified by fitting the autocorrelation function of the signal, without vibration.

Two main difficulties had to be resolved. In the pulsed mode, we had to overcome the saturation of the electrical amplification chain for high signal peak power, which originally saturated the CNR at 10 dB. Also, parasitic vibrations of the speckle generating disk (including a broadband component that particularly impacted on the ML estimator, which assumes

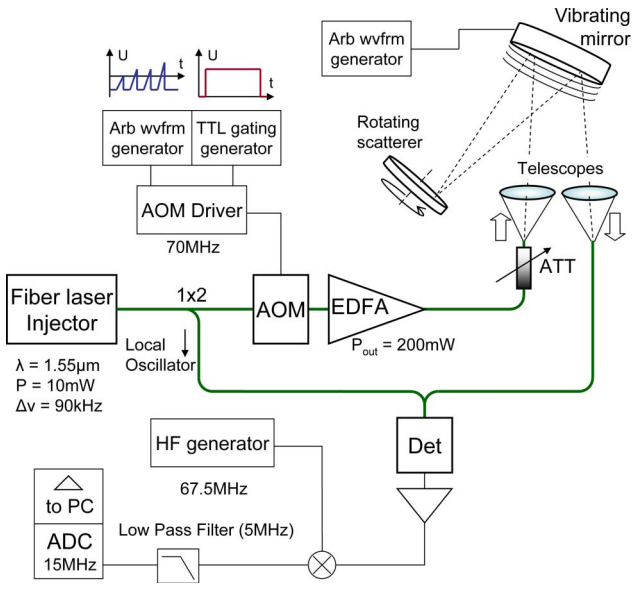

Fig. 8. (Color online) Diagram of experimental apparatus allowing CW and polypulse operations. A rotating scatterer is used to create speckle noise with bandwidth $B_{\text{speckle}} = 5$ kHz: EDFA, erbium-doped fiber amplifier; ATT, attenuator; Det, detector; HF, high frequency; ADC, analog-to-digital converter).

stationary IF during the waveform) had to be minimized, which was done by using lower rotation rates and larger spot sizes and, thus, a larger vibrating mirror. These parasitic vibrations were reduced by a factor of 2 but could not be entirely suppressed; the following experimental results include this artifact.

B. Results

Figure 9 summarizes the results of this experimental comparison of waveforms and signal processing methods, with SNR versus CNR curves for the best methods found in the previous section (top) and average vibration spectra at high CNR (bottom).

Figure 9 (bottom) shows the vibration spectra averaged on 20 to 40 runs of 1 s each at the highest CNR achieved for each waveform. We see the vibration is fine-tuned to be almost identical to that used in the simulations (see Fig. 5).

The SNR versus CNR curves on Fig. 9 (top) follow the typical increasing trend with a plateau at high CNR, when velocity precision becomes speckle limited. However, parasitic vibrations cause this SNR saturation to occur about 3 dB lower than in the simulation. At a low CNR, we find the expected SNR fall as CNR^2 for SGC and as CNR for pulse-pair vibrometry, as demonstrated in [7].

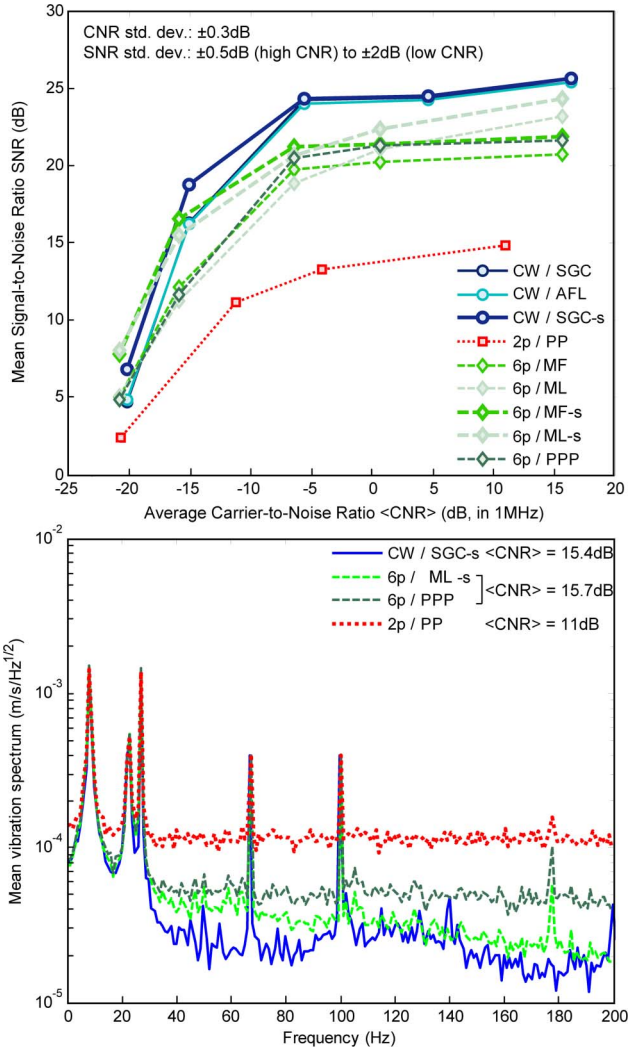

Fig. 9. (Color online) Experimental SNR plotted as a function of CNR (top) and experimental spectra at high CNR (bottom), averaged over 20 to 40 measurements, for CW, pulse pairs ($2p$), and six-pulse waveforms ($6p$).

Overall, the simulation results are corroborated, including the better performance of the ML estimator at a high CNR, compared to the more classical PPP or MF processing. Six-pulse waveforms are clearly more successful than pulse pairs in these conditions. This is also seen by comparing the vibration spectra obtained at a high CNR in Fig. 9 (bottom). However, experimental artifacts make the gain in SNR of the ML estimator less important than in simulation. It is also noticeable that this gain does not become interesting unless the CNR is above 5 dB, and after that threshold it increases linearly, as simulations showed. Unfortunately, as a CNR over 20 dB is difficult to obtain, very important gains due to the use of ML over regular IF estimators cannot be relied upon in practice.

Yet the SNR increase due to TFR smoothing, which nears 5 dB in some cases, was not expected to persist at such high CNR values in the pulsed mode. It is still measurable when the signal is fairly strong, which means that the impact of signal fading is underestimated in our simulation and that TFR smoothing is indeed helpful in the pulsed mode, when velocity measurements are few.

7. Conclusion

We have presented and qualified advanced signal processing techniques applicable to pulsed laser vibrometry with polypulse waveforms, to enhance the determination of the modal frequencies of a remote target in harsh noise conditions. This work focuses on what we believe is the first extensive comparison between these waveforms and processing methods, particularly in the case when this measurement is made difficult by strong decorrelation noise such as target speckle noise. It can, indeed, reduce the interest of pulsed vibrometry, for instance when compared to classical CW vibrometry, which averages numerous velocity measurements. An additional hypothesis is taken: an equal mean laser power to be distributed between emitted waveforms.

In this framework, polypulse waveforms do not have peak power as high as the first employed pulse pairs and will not present as much gain at a very long range. But because of their longer effective duration when the pulse separation is set to avoid Doppler ambiguities, every test presented here has proved them more robust in the said noise conditions. Because it did not exist in pulsed mode, a specific processing based on ML IF estimation, which takes into account what we know of the noise statistics, has been developed. By comparing the velocity precision of this processing method to its theoretical limits (CRB), it has been shown that it is closer to optimal than that of simple polypulse-pair processing. Also, we have proposed TFRs, already applied in CW vibrometry, and show that they can be of

use for noise regularization in pulsed vibrometry, for instance, by temporal smoothing.

A comprehensive comparison of the SNR performance of the described processing to that of classical methods, for vibrometry with pulsed and CW emission, has been conducted on simulated signals and later confirmed by experimentation. The first conclusion is that advanced processing, based on the TFR of the likelihood as a function of the IF for each waveform, with an additional temporal smoothing of this TFR, gives the best result in pulsed vibrometry, especially with dominant speckle, with no additional computational cost. Secondly, in case of weak signals (low CNR), at long range for instance, temporal smoothing of TFR proved useful as a noise regularization. Moreover, in the case of mismatched analysis bandwidth, pulsed vibrometry with polypulse waveforms and matched filtering was finally shown to be more robust than CW vibrometry with SGC demodulation. This is in spite of the strong speckle noise that was impacting the signal.

However, these results are tempered by the high CNR required for the developed estimator to obtain a gain in SNR and its sensitivity to deviations from the model assumed in Section 2 of this article. As has been proven by our experiment, high-frequency vibrations are enough to decrease its performance, because it assumes stationary IF during the velocity measurement time T_m. This defect could nevertheless be acted upon by including the possibility of IF drift in the model. Another issue of the current study is that, by assuming the same average laser power for each emission mode, it allowed a general comparison but failed to take into account technological limitations. For instance, fiber lasers at $1.55\,\mu$m with a MOPA configuration, such as the one we used, are instead limited by the peak power or the energy accumulated in the amplifying fiber. A direct sequel of this study will be to evaluate the actual optimal performance of such a fibered vibrometer.

The results of this work still push toward the use of longer waveforms, of estimators that take into account signal statistics, and of TFR regularization in pulsed vibrometry. Further advances can be made in each of these three directions. With sufficiently resilient ambiguity resolving algorithms, and assuming suitable emission architecture, staggered polypulses can achieve very large measurement dynamics. Also, ML based parametric estimators, including a complete model of the vibration, remain the optimal processing method if the computational load is not prohibitive, despite the many parameters required for it to be robust. Finally, if the latter improvements are not possible, the vibration can still be better estimated from a TFR, by taking advantage of the signal continuity in the time-frequency space.

Our future works will involve studying such techniques for IF tracking on TFRs and developing parametric estimation for other applications of vibrometry.

We thank Christopher Hill from QinetiQ as well as Matthieu Valla and Guillaume Canat from Onera for useful discussions and Didier Goular and Béatrice Augère from Onera for technical support. This work was partly supported by the Délégation Générale de l'Armement, Mission pour la Recherche et l'Innovation Scientifique.

References

1. P. Gueguen, V. Jolivet, C. Michel, and A.-S. Schveitzer, "Comparison of velocimeter and coherent lidar measurements for building frequency assessment," Bull. Earthquake Eng. **8**, 327–338 (2010).
2. W. Kranz, "Target classification by laser vibration sensing," Proc. SPIE **1181**, 301–306 (1989).
3. S. M. Hannon, J. A. Thomson, S. W. Henderson, P. Gatt, R. Stoneman, and D. Bruns, "Agile multiple pulse coherent lidar for range and micro-Doppler measurement," Proc. SPIE **3380**, 259–269 (1998).
4. P. Gatt, S. W. Henderson, and B. Krause, "Poly-pulse coherent lidar waveforms for coherent lidar measurements," presented at the Coherent Optical Technologies and Applications Conference, Whistler, Canada, 25 June 2006.
5. S. W. Henderson, J. A. Thomson, S. M. Hannon, and P. Gatt, "Comparison of pulsed waveform and CW lidar for remote vibration measurement," presented at the 10th Coherent Laser Radar Conference, Mount Hood, Oregon, 28 June 1999.
6. C. Hill, M. Harris, and K. D. Ridley, "Fiber-based $1.5\,\mu$m lidar vibrometer in pulsed and continuous modes," Appl. Opt. **46**, 4376–4385 (2007).
7. P. Gatt, S. W. Henderson, and S. M. Hannon, "Noise mechanisms impacting micro-Doppler lidar signals: theory and experiment" Tech. Rep. (Coherent Technologies, Incorporated, 2000).
8. C. Hill, M. Harris, K. D. Ridley, E. Jakeman, and P. Lutzmann, "Lidar frequency modulation vibrometry in the presence of speckle," Appl. Opt. **42**, 1091–1100 (2003).
9. A. Ishimaru, "The beam wave case and remote sensing," in *Topics in Applied Physics 25: Laser Beam Propagation in the Atmosphere*, J. W. Strohbehn, ed. (Springer, 1978), pp. 129–170.
10. A. L. Kachelmyer and K. I. Schultz, "Spectrogram processing of laser vibration data," Proc. SPIE **1936**, 78–88 (1993).
11. D. G. Youmans, "Joint time-frequency transform processing for linear and sinusoidal FM coherent ladars," Proc. SPIE **5087**, 46–57 (2003).
12. W. F. Buell, B. A. Shadwick, and R. W. Farley, "Bayesian spectrum analysis for laser vibrometry processing," Tech. Rep. (Institute for Advanced Physics, 2000).
13. B. J. Rye and R. M. Hardesty, "Discrete spectral peak estimation in incoherent backscatter heterodyne lidar," IEEE Trans. Geosci. Remote Sensing **31**, 16–35 (1993).
14. D. G. Youmans, "Target spectral estimation using direct detection and coherent detection ladar," Proc. SPIE **5791**, 97–108 (2005).
15. B. C. Lovell and R. C. Williamson, "The statistical performance of some instantaneous frequency estimators," IEEE Trans. Signal Process. **40**, 1708–1723 (1992).
16. M. Ghogho, A. K. Nandi, and A. Swami, "Cramér-Rao bounds and maximum likelihood estimation for random amplitude phase-modulated signals," IEEE Trans. Signal Process. **49**, 2905–2916 (2001).
17. J.-P. Tourrenc, P. Signoret, M. Myara, M. Bellon, J.-P. Perez, J.-M. Gosalbes, R. Alabedra, and B. Orsal, "Low-frequency FM-noise-induced lineshape: a theoretical and experimental approach," IEEE J. Quantum Electron. **41**, 549–553 (2005).
18. C. Spiegelberg, J. Geng, Y. Hu, Y. Kaneda, S. Jiang, and N. Peyghambarian, "Low-noise narrow-linewidth fiber laser at 1550 nm," J. Lightwave Technol. **22**, 57–62 (2004).

19. O. Michel, A. Hero, and P. Flandrin, "Graphes de représentation minimaux, entropies et divergences: applications," Traitement du Signal **17**, 287–297 (2000).
20. T. Thayaparan, L. Stankovic, I. Djurovic, S. Penamati, and K. Venkataramaniah, "Intelligent target recognition using micro-Doppler radar signatures," Proc. SPIE **7308**, 17–28 (2009).
21. D. N. Schimpf and C. Ruchert, "Compensation of pulse-distortion in saturated laser amplifiers," Opt. Express **16**, 17637–17646 (2008).